NANO LETTERS

pubs.acs.org/NanoLett

Letter

Anisotropic Transient Disordering of Colloidal, Two-Dimensional CdSe Nanoplatelets upon Optical Excitation

Alexandra Brumberg, Matthew S. Kirschner, Benjamin T. Diroll, Kali R. Williams, Nathan C. Flanders, Samantha M. Harvey, Ariel A. Leonard, Nicolas E. Watkins, Cunming Liu, Eli D. Kinigstein, Jin Yu, Austin M. Evans, Yuzi Liu, Shelby A. Cuthriell, Shobhana Panuganti, William R. Dichtel, Mercouri G. Kanatzidis, Michael R. Wasielewski, Xiaoyi Zhang, Lin X. Chen, and Richard D. Schaller*

Cite This: *Nano Lett.* 2021, 21, 1288−1294

Read Online

ACCESS | Metrics & More | Article Recommendations | Supporting Information

ABSTRACT: Nanoplatelets (NPLs)—colloidally synthesized, spatially anisotropic, two-dimensional semiconductor quantum wells—are of intense interest owing to exceptionally narrow transition line widths, coupled with solution processability and bandgap tunability. However, given large surface areas and undercoordinated bonding at facet corners and edges, excitation under sufficient intensities may induce anisotropic structural instabilities that impact desired properties. We employ time-resolved X-ray diffraction to study the crystal structure of CdSe NPLs in response to optical excitation. Photoexcitation induces greater out-of-plane than in-plane disordering in 4 and 5 monolayer (ML) NPLs, while 3 ML NPLs display the opposite behavior. Recovery dynamics suggest that out-of-plane cooling slightly outpaces in-plane cooling in 5 ML NPLs with recrystallization occurring on indistinguishable time scales. In comparison, for zero-dimensional CdSe nanocrystals, disordering is isotropic and recovery is faster. These results favor the use of NPLs in optoelectronic applications, where they are likely to exhibit superior performance over traditional, zero-dimensional nanocrystals.

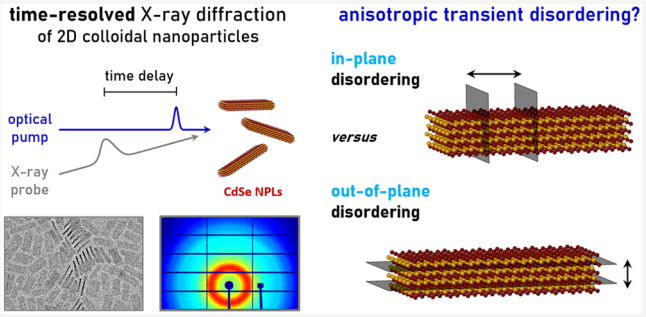

KEYWORDS: *Nanoplatelets, nonequilibrium phenomena, transient heating, X-ray diffraction, anisotropic disordering*

Downloaded via ARGONNE NATL LABORATORY on September 4, 2021 at 16:10:56 (UTC).
See https://pubs.acs.org/sharingguidelines for options on how to legitimately share published articles.

Two-dimensional materials, such as transition metal dichalcogenides, black phosphorus, and graphene, present remarkable properties that arise from their structures, which pair spatial extension in the lateral plane with quantum confinement.[1−3] As a result, 2D semiconductors have received significant attention for atomic-scale transistors, photocatalysts, spintronics, and optoelectronics.[1,4−7] The promise of 2D colloidal nanomaterials such as nanoplatelets (NPLs) likewise stems from their spatially extended lattices, coupled with the benefits of tunable electronic bandgap and solution processability of well-defined structures whose properties do not depend on the selected substrate. The NPL bandgap can be tuned via the number of unit cells comprising the particle thickness,[8−13] ligand identity,[14−17] or composition (such as the growth of a semiconductor shell or crown[18−20] or compositional alloying[21,22]). As a result of quantum confinement in one dimension paired with spatially extended morphology, NPLs exhibit nearly homogeneous ensemble emission line widths,[8,23] large absorption cross sections,[24,25] and reduced rates of Auger recombination[26,27] compared to zero-dimensional nanocrystals (NCs). Notably, these features have led to the development of high-performance light-emitting diodes (LEDs)[28,29] and nanoscale lasers with low gain thresholds.[26,30] Although these devices subject the optically active layer to high intensity excitation, the potential of such conditions to engender structural modifications in NPLs is not known.

Following photoexcitation or electrical injection, deposited energy in excess of the band gap heats the lattice through electron−phonon coupling.[31,32] Under low carrier loads, lattice heating is typically negligible; however, at high carrier injection conditions, such as those used in high current LEDs or lasers, lattice heating becomes significant enough to potentially impact structure and device performance.[33−35] In NCs, heat deposition is particularly consequential, as finite lattice sizes and large surface-to-volume ratios reduce thermal conductivity[36] and reduce melting points via increased surface energy.[37−39] In highly anisotropic structures such as 2D colloidal NPLs, large, flat facets appear, but the presence of higher surface energy

Received: October 2, 2020
Revised: December 29, 2020
Published: January 19, 2021

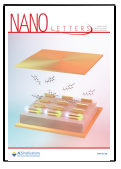

ACS Publications

© 2021 The Authors. Published by American Chemical Society

https://dx.doi.org/10.1021/acs.nanolett.0c03958
Nano Lett. 2021, 21, 1288−1294

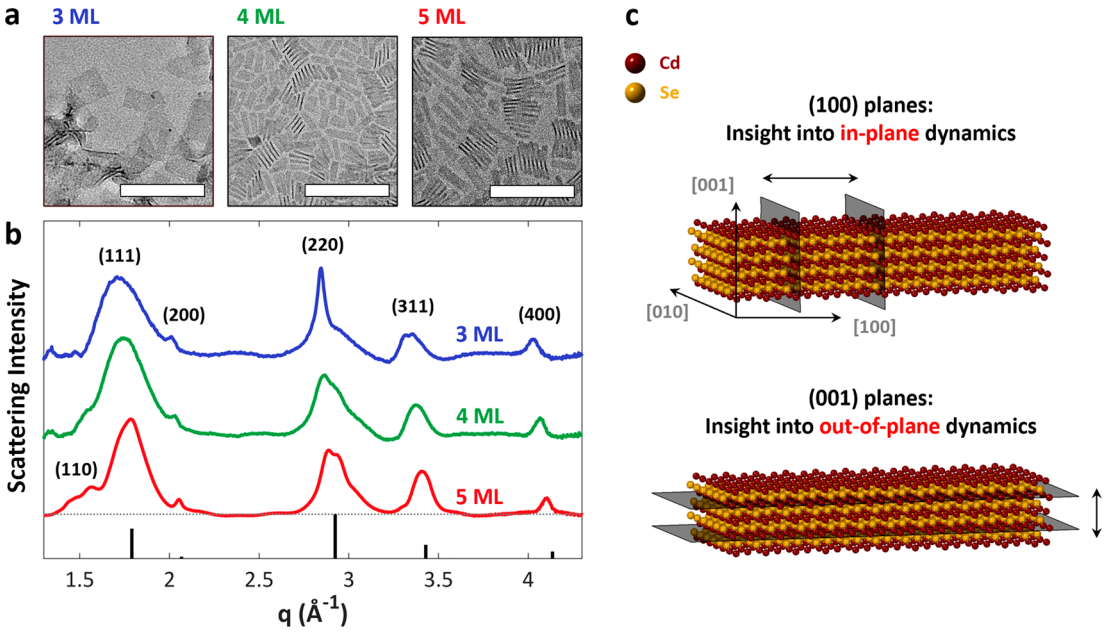

Figure 1. Static characterization of CdSe nanoplatelets. (a) Transmission electron microscopy images of 3, 4, and 5 ML CdSe NPLs. Scale bars are 100 nm. (b) Baseline-subtracted static X-ray diffraction patterns of 3, 4, and 5 ML CdSe NPLs dispersed in solvent (dodecane for 3 and 4 ML, heptamethylnonane for 5 ML) at 30 °C. For reference, the bulk zinc blende CdSe diffraction pattern is shown in black below the experimental data (ICSD 41528). (c) Schematic of a 4 ML zinc blende CdSe NPL, showing alternating layers of Cd and Se stacked along the [001] direction. In-plane dynamics can be observed by monitoring the response of the (100) planes after photoexcitation, whereas out-of-plane dynamics can be obtained from the response of the (001) planes.

corners and edges may confer greater susceptibility to melting.[40,41] Ultrafast electron diffraction and X-ray scattering studies of 2D materials physically grown on substrates have revealed anisotropic responses following photoexcitation with large atomic displacements and wrinkling of the layers following photoexcitation.[42−44] Because NC structure and shape dictate electronic structure, effects such as rippling of 2D materials can impact bandgap and related optoelectronic properties.[45,46]

Here, we study the response of colloidal NPL crystal structure upon optical excitation using time-resolved X-ray diffraction (TR-XRD). TR-XRD has previously been used to measure transient structural responses to ultrafast optical excitation in semiconductor NCs, revealing effects such as thermal expansion, disordering of the crystal lattice, and phase transitions.[33,34,47−50] Using three thicknesses of CdSe NPLs, we show that intense optical excitation induces anisotropic disordering of the NPL lattice with more significant out-of-plane than in-plane disordering in 4 and 5 ML NPLs, and the opposite effect in 3 ML NPLs. Recovery dynamics in 5 ML NPLs are also probed, revealing slightly faster out-of-plane than in-plane cooling, and overall slower recovery dynamics than in quasi-spherical CdSe NCs.

CdSe NPLs of three different thicknesses, shown via transmission electron microscopy (TEM) in Figure 1a and UV−Vis absorption in Figure S1, were synthesized according to previously published procedures.[8,26] In the thickness (or z) direction, NPLs are composed of n alternating monolayers (ML) of Cd and Se (n = 3, 4, 5) and terminated by one final layer of Cd to achieve NPLs that measure 0.9, 1.2, and 1.5 nm in thickness, respectively. Lateral sizes measure 37 nm × 67 nm, 7.4 nm × 23 nm, and 7.6 nm × 41 nm for 3, 4, and 5 ML NPLs, respectively (see also Supporting Information Table S1). Oleate ligands passivate the Cd^{2+}-terminated surfaces. Atoms pack in a tetragonally distorted zinc blende crystal structure,[14] giving rise to the static XRD patterns shown in Figure 1b. Tetragonal distortion manifests in the appearance of the forbidden (110) peak and via multiple components in the (220) peak family, which arise from expansion of the lattice laterally (in the x- and y-directions) and contraction vertically (in the z-direction).[14,51,52] More distortion in thinner NPLs, along with different aspect ratios, result in distinct (220) line shapes for the different NPL thicknesses. NPL thickness increases along the [001] axis, as shown in Figure 1c, such that the large NPL lateral surfaces are composed of (001) planes. Because of Scherrer broadening that arises from reduced unit cell repeats in small crystals, the sharp (400) diffraction peak arises primarily from planes that repeat along the length of the NPL in the longest direction (the [100] axis, or x-direction). Contributions from the (040) and (004) planes, repeating along the much shorter [010] and [001] axes, are likely too weak and too broad to be observed. Similarly, diffraction from (220) planes in the xy plane (parallel to the thickness, or z, direction) is sharp, compared to the convolved, broader (202) and (022) planes (see Figure S3). The (400) diffraction peak thus provides insight into in-plane dynamics along the lateral extent of the NPL, whereas both in-plane and out-of-plane dynamics are revealed via analysis of the (220) peak family.

To investigate the impact that photoexcitation at elevated fluences imparts on NPL structure, we employed TR-XRD at Beamline 11-ID-D of the Advanced Photon Source (Argonne National Laboratory) as illustrated in Figure S4. NPLs dispersed in dodecane were photoexcited by 1.6 ps, 400 nm (3.1 eV) pump pulses at 10 kHz and probed at fixed delay times by 79 ps, 11.72 keV X-ray probe pulses. The transient scattering X-ray response, ΔS, was isolated by subtracting the diffraction pattern prior to photoexcitation from that after photoexcitation (see the Supporting Information for details regarding data processing).

Figure 2a shows TR-XRD patterns for 5 ML CdSe NPLs at 40 ps, the time delay with the strongest observed transient

https://dx.doi.org/10.1021/acs.nanolett.0c03958
Nano Lett. 2021, 21, 1288−1294

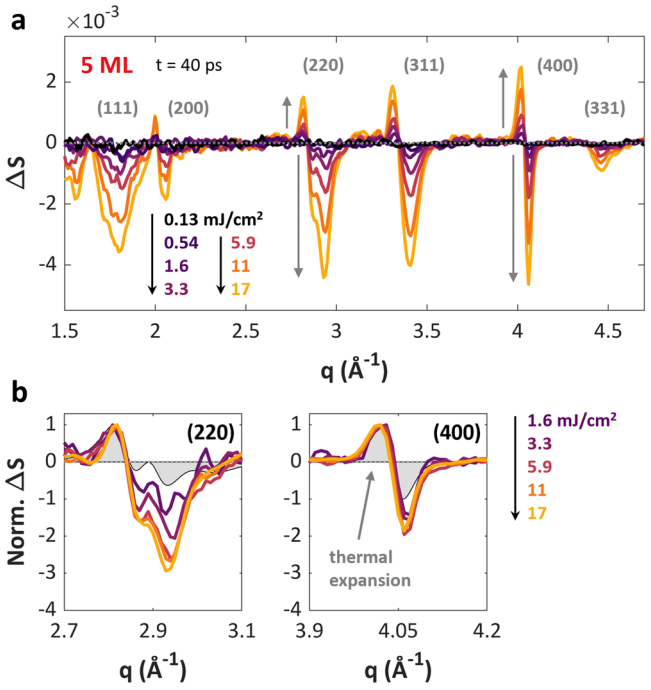

Figure 2. Time-resolved X-ray diffraction of 5 ML CdSe NPLs, 40 ps after photoexcitation. (a) TR-XRD patterns as a function of increasing fluence. (b) TR-XRD patterns, normalized to a maximum of 1, for the (220) and (400) peaks. The area shaded in gray represents the TR-XRD pattern that results from only a peak shift to lower q (i.e., thermal expansion). Deviations from this line shape arise from loss in diffraction due to transient disordering.

response. Inspection of the TR-XRD line shape for each diffraction peak reveals the extent to which crystalline planes transiently disorder after photoexcitation. Thermal expansion only, with no disordering, shifts diffraction peaks to lower q values, resulting in the TR-XRD patterns highlighted in Figure 2b in gray. (Temperature-dependent static X-ray diffraction measurements of 5 ML CdSe NPLs, presented in Figure S7, do not show the decrease in scattering intensity with q^2 as expected from Debye−Waller theory.) The (400) peak deviates only minimally from this line shape, pointing to in-plane thermal expansion with minimal in-plane disordering on the time scale of this experiment. In contrast, the (220) peak family presents more prominent negative features, signaling loss in diffraction intensity that arises from significant out-of-plane disordering, possibly consistent with buckling that decreases out-of-plane unit cell registry.

As shown in Figure 2b, the excitation fluence dependence of these two peaks is also anisotropic. Although the line shape of the (400) peak remains relatively unchanged between 1.6 and 17 mJ/cm^2, the (220) peak family progressively loses more scattering intensity. This behavior suggests fairly constant in-plane disordering with marginal fluence dependence, in contrast to the strongly fluence-dependent out-of-plane disordering (see also Figure S8). Notably, out-of-plane disordering may lead to undesirable changes in electronic properties (such as transition line width), as NPL thickness dominates these characteristics.

Such anisotropic response to photoexcitation is not present in quasi-spherical wurtzite[33] or quasi-spherical zinc blende CdSe NCs, which both display isotropic changes to the lattice, as well as substantial disordering at comparable fluences (see Figure S9). Furthermore, the relative lack of in-plane disordering in CdSe NPLs even at elevated fluences suggests that CdSe NPLs are more robust to optical excitation than quasi-spherical CdSe NCs. The highest fluence probed here of 17 mJ/cm^2 corresponds to an average of 4 excitons/nm^3 (based on an absorption cross-section of 4 × 10^{-14} cm^2; see Supporting Information for details), yet NPLs retain in-plane crystallinity. This is in contrast to quasi-spherical CdSe NCs, which exhibit extensive disordering (akin to melting) at exciton densities above 1 exciton/nm^3.[33] This is likely due to the prominence of flat faces over much of the NPL surface, in comparison to the highly convex surfaces of quasi-spherical NCs.

Figure 3 displays normalized TR-XRD patterns of the (220) and (400) peaks for 3, 4, and 5 ML NPLs (see also Figure S10).

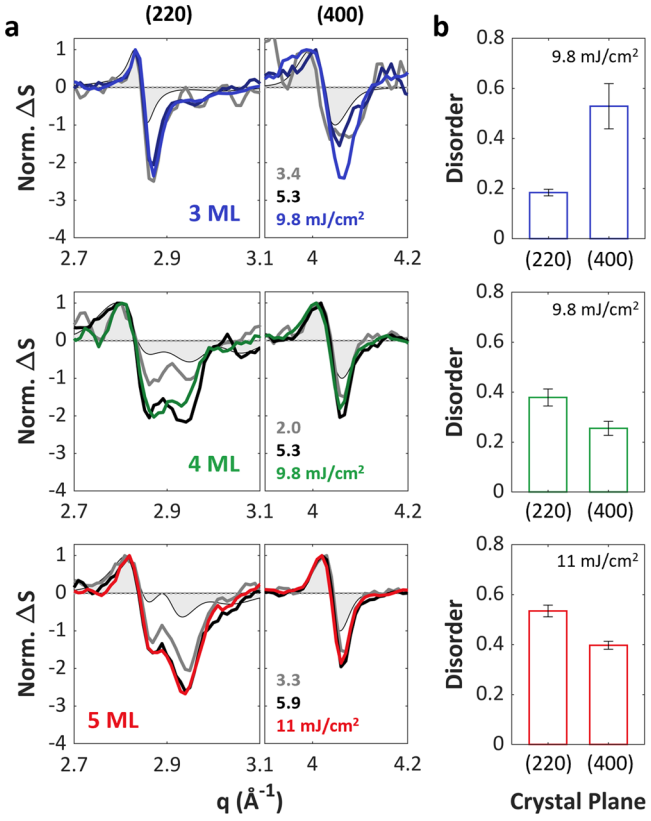

Figure 3. Thickness dependence of NPL thermal response. (a) TR-XRD patterns, normalized to a maximum of 1, of the (220) and (400) peaks 40 ps after excitation for 3, 4, and 5 ML NPLs at comparable fluences. The areas shaded in gray represent the TR-XRD patterns that result from only a peak shift to lower q (i.e., thermal expansion). (b) Fraction of the integrated |ΔS| peak area that stems from transient disordering for the (220) versus (400) planes at ∼10 mJ/cm^2 for each thickness.

As the NPL thickness increases, the response of the (220) peak family changes in accordance with the differing distributions of the (220), (202), and (022) components observed in static diffraction (Figure 1b). Interestingly, the 3 ML sample exhibits disordering in the (220) plane at all examined powers, possibly due to the enhanced flexibility of the thinner structures. As shown in Figure S11, the lowest power at which we discern changes in scattering intensity (1 mJ/cm^2) in the (220) peak family features the same extent of disordering as observed at higher studied fluences. This is markedly different than the previously observed behavior for quasi-spherical CdSe NCs,[33]

https://dx.doi.org/10.1021/acs.nanolett.0c03958
Nano Lett. 2021, 21, 1288−1294

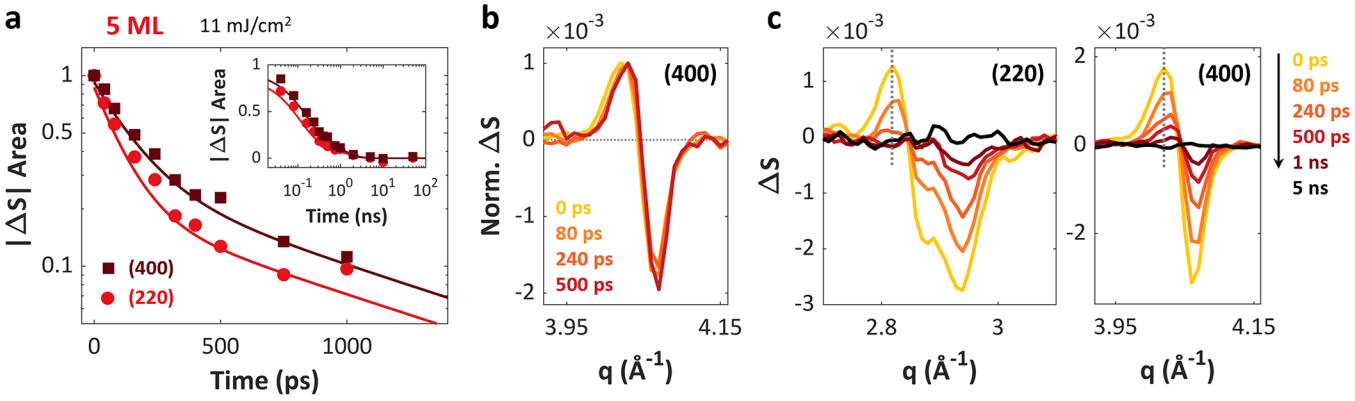

Figure 4. Cooling and recrystallization dynamics of 5 ML CdSe NPLs. (a) Recovery dynamics in 5 ML NPLs after 400 nm excitation at 11 mJ/cm^2, determined by integrating |ΔS| for each peak. For each curve, dynamics is normalized to 1. Solid lines are biexponential fits to the data. Inset shows fit to longer time delays. (b) TR-XRD of the (400) peak at four different time points early in the recovery process, normalized to a maximum value of 1. No change in line shape is apparent. (c) TR-XRD patterns of the (220) and (400) peaks up to 5 ns after photoexcitation.

where thermal expansion is the dominant response at low powers and disordering only arises with increasing fluence.

To quantify the extent of disordering in each plane as a function of NPL thickness, in Figure 3b we plot the fraction of the integrated peak area that stems from transient disordering for the (220) versus (400) peaks at ∼10 mJ/cm^2, which corresponds to ∼2−3 excitons/nm^3 in all three samples. The area that arises from disordering is quantified as the component that cannot be attributed to the gray shaded area in Figure 3a arising from thermal expansion. Consistent with the qualitative results obtained from Figure 2b, Figure 3b shows that disordering for 5 ML NPLs is anisotropic. In the (400) direction, disordering contributes to 40 ± 2% of the peak area, while disordering contributes to 53 ± 2% of the peak area in the (220) direction. Four ML NPLs display similar trends, suggesting that thick NPLs respond to photoexcitation anisotropically with more pronounced disordering in the out-of-plane direction. On the other hand, disordering only contributes to 18 ± 1% of the (220) peak area for 3 ML NPLs, compared to 53 ± 9% for the (400) plane. Thinner NPLs thus display anisotropic disordering in an opposite manner, with stronger in-plane disordering, perhaps because of their enhanced flexibility.

Recovery dynamics of the 5 ML diffraction peaks, generated by integrating the absolute value of the change in scattering intensity at each diffraction peak as a function of delay time, are plotted in Figure 4a. Analysis of recovery dynamics yields information regarding the time scales of both cooling (the reversal of thermal expansion) and recrystallization (the reversal of disordering). Indeed, as shown in Figure 4a, recovery appears biexponential with τ_1 requiring about 100 ps and τ_2 occurring on a nanosecond time scale (see Table S5 for fits). Though admittedly not outside error bars, a slight difference in fitted τ_1 values appears to exist, as the (220) peak family recovers with τ_1 = 107 ± 29 ps while the (400) peak recovers with τ_1 = 147 ± 42 ps. Since the (220) peak family dynamics probe both in-plane and out-of-plane recovery, these lifetimes point to potentially anisotropic recovery dynamics, with faster out-of-plane cooling. This can perhaps be attributed to shorter distances and more rapid surface scattering in the out-of-plane direction compared to the in-plane direction. The second, slower recovery component of $\tau_2 \approx 1$ ns is attributed to slower dissipation at the surface/ligand interface. Notably, complete recovery in CdSe NPLs is much slower than that of quasi-spherical CdSe NCs, where the latter cool and recrystallize within a few hundred picoseconds.[33]

TR-XRD line shape during recovery aids assignment of the two lifetimes to cooling versus recrystallization. Figure 4b displays normalized transient diffraction patterns for the 5 ML (400) peak following photoexcitation, whereas Figure 4c displays un-normalized transient diffraction patterns for both the (220) and (400) peaks. Over the first 500 ps following photoexcitation, the degree of disordering (i.e., the peak line shape) in the (400) peak displayed in Figure 4b remains unchanged, suggesting that any recrystallization thus far is minor. Instead, the disappearance of the (220) peak positive component and the shift of the (400) peak to progressively higher q-values in Figure 4c indicate that the fast component of the recovery dynamics corresponds to cooling. Recrystallization occurs over nanoseconds, as evidenced by the loss of diffraction intensity due to disordering remaining past 1 ns.

In conclusion, we have shown that CdSe NPL lattices respond anisotropically to controlled fluence optical excitation. Following excitation, the crystal lattice undergoes both thermal expansion and disordering, but to different degrees along different axes. Out-of-plane disordering is more significant than in-plane disordering for 4 and 5 ML NPLs, whereas the opposite holds true for thinner 3 ML NPLs. These findings offer significant implications for optoelectronic devices, where the ability to operate at high excitation densities without loss of tailored properties is advantageous. In particular, out-of-plane disordering in NPLs could lead to changes in the bandgap, resulting in lower color gamut in LEDs or detrimental transition line broadening effects in lasing.[53] Together, these results suggest that both NC composition and structure influence crystal lattice stability and resulting optical performance.

■ ASSOCIATED CONTENT

Supporting Information

The Supporting Information is available free of charge at https://pubs.acs.org/doi/10.1021/acs.nanolett.0c03958.

Sample details (synthesis, UV−Vis spectra, transmission electron microscopy, additional discussion regarding the crystal structure, and absorption cross-sections); experimental methods and data processing of time-resolved X-ray diffraction data; calculation of heating-only TR-XRD patterns; and supplementary data (temperature-dependent static X-ray diffraction used to evaluate Debye−Waller

https://dx.doi.org/10.1021/acs.nanolett.0c03958
Nano Lett. 2021, 21, 1288−1294

effects, fluence-dependent data for spherical CdSe NCs, fluence-dependent data for 3 and 4 ML CdSe NPLs, fluence-dependent data for in-plane and out-of-plane disordering, and fitted recovery dynamics for 3 and 5 ML CdSe NPLs) (PDF)

AUTHOR INFORMATION

Corresponding Author

Richard D. Schaller − *Department of Chemistry and Institute for Sustainability and Energy at Northwestern, Northwestern University, Evanston, Illinois 60208, United States; Center for Nanoscale Materials, Argonne National Laboratory, Lemont, Illinois 60439, United States;* orcid.org/0000-0001-9696-8830; Email: schaller@northwestern.edu, schaller@anl.gov

Authors

Alexandra Brumberg − *Department of Chemistry, Northwestern University, Evanston, Illinois 60208, United States;* orcid.org/0000-0003-2512-4686

Matthew S. Kirschner − *Department of Chemistry, Northwestern University, Evanston, Illinois 60208, United States;* orcid.org/0000-0001-6849-4869

Benjamin T. Diroll − *Center for Nanoscale Materials, Argonne National Laboratory, Lemont, Illinois 60439, United States;* orcid.org/0000-0003-3488-0213

Kali R. Williams − *Department of Chemistry, Northwestern University, Evanston, Illinois 60208, United States*

Nathan C. Flanders − *Department of Chemistry, Northwestern University, Evanston, Illinois 60208, United States*

Samantha M. Harvey − *Department of Chemistry and Institute for Sustainability and Energy at Northwestern, Northwestern University, Evanston, Illinois 60208, United States*

Ariel A. Leonard − *Department of Chemistry, Northwestern University, Evanston, Illinois 60208, United States*

Nicolas E. Watkins − *Department of Chemistry, Northwestern University, Evanston, Illinois 60208, United States*

Cunming Liu − *X-ray Science Division, Argonne National Laboratory, Lemont, Illinois 60439, United States*

Eli D. Kinigstein − *X-ray Science Division, Argonne National Laboratory, Lemont, Illinois 60439, United States*

Jin Yu − *X-ray Science Division, Argonne National Laboratory, Lemont, Illinois 60439, United States*

Austin M. Evans − *Department of Chemistry, Northwestern University, Evanston, Illinois 60208, United States;* orcid.org/0000-0002-3597-2454

Yuzi Liu − *Center for Nanoscale Materials, Argonne National Laboratory, Lemont, Illinois 60439, United States;* orcid.org/0000-0002-8733-1683

Shelby A. Cuthriell − *Department of Chemistry, Northwestern University, Evanston, Illinois 60208, United States*

Shobhana Panuganti − *Department of Chemistry, Northwestern University, Evanston, Illinois 60208, United States;* orcid.org/0000-0003-1762-527X

William R. Dichtel − *Department of Chemistry, Northwestern University, Evanston, Illinois 60208, United States;* orcid.org/0000-0002-3635-6119

Mercouri G. Kanatzidis − *Department of Chemistry and Institute for Sustainability and Energy at Northwestern, Northwestern University, Evanston, Illinois 60208, United States;* orcid.org/0000-0003-2037-4168

Michael R. Wasielewski − *Department of Chemistry and Institute for Sustainability and Energy at Northwestern, Northwestern University, Evanston, Illinois 60208, United States;* orcid.org/0000-0003-2920-5440

Xiaoyi Zhang − *X-ray Science Division, Argonne National Laboratory, Lemont, Illinois 60439, United States;* orcid.org/0000-0001-9732-1449

Lin X. Chen − *Department of Chemistry and Institute for Sustainability and Energy at Northwestern, Northwestern University, Evanston, Illinois 60208, United States; Chemical Science and Engineering, Argonne National Laboratory, Lemont, Illinois 60439, United States;* orcid.org/0000-0002-8450-6687

Complete contact information is available at: https://pubs.acs.org/10.1021/acs.nanolett.0c03958

Author Contributions

A.B., M.S.K., S.M.H., A.A.L., N.E.W., N.C.F., S.A.C., S.P., C.L., J.Y., E.D.K., X.Z., and R.D.S. conducted TR-XRD experiments. B.T.D. and K.R.W. synthesized the NPLs. B.T.D. and Y.L. collected electron microscopy images. N.C.F. and A.M.E. conducted temperature-dependent static XRD. A.B. and M.S.K. contributed to data processing and analysis. All authors contributed to the writing of this manuscript.

Notes

The authors declare no competing financial interest.

ACKNOWLEDGMENTS

The authors thank D. C. Hannah, M. J. Wagner, D. Hayes, A. Y. Chang, and C. E. Rowland for their assistance in collecting TR-XRD data on quasi-spherical zinc blende CdSe NCs as well as W. Ji and A. Natraj for their assistance in conducting static XRD on CdSe NPLs. This material is based upon work supported by the National Science Foundation under Grants 1629383 and 1808590, as well as by the National Science Foundation Graduate Research Fellowship Program under Grant DGE-1842165 (A.B., S.M.H., N.E.W., A.M.E., and S.P.). This work was supported by the U.S. Department of Energy, Office of Science, Office of Basic Energy Sciences under Award DE-FG02-99ER14999 (M.R.W.). A.B. gratefully acknowledges support from a 3M Graduate Research Fellowship, the Ryan Fellowship, and the International Institute for Nanotechnology at Northwestern University. This research used resources of the Advanced Photon Source, a U.S. Department of Energy (DOE) Office of Science User Facilities operated by Argonne National Laboratory under Contract No. DE-AC02-06CH11357. Use of the Center for Nanoscale Materials, an Office of Science user facility, was supported by the U.S. Department of Energy, Office of Science, Office of Basic Energy Sciences, under Contract No. DE-AC02-06CH11357. A.A.L., M.S.K., and L.X.C. are partially supported by the Ultrafast Initiative of the U.S. Department of Energy, Office of Science, Office of Basic Energy Sciences, through Argonne National Laboratory under Contract No. DE-AC02-06CH11357. Parts of this work were performed at the DuPont-Northwestern-Dow Collaborative Access Team (DND-CAT) located at Sector 5 of the Advanced Photon Source (APS). DND-CAT is supported by Northwestern University, E.I. DuPont de Nemours & Co., and the Dow Chemical Company.

REFERENCES

(1) Manzeli, S.; Ovchinnikov, D.; Pasquier, D.; Yazyev, O. V.; Kis, A. 2D Transition Metal Dichalcogenides. *Nat. Rev. Mater.* **2017**, *2* (8), 17033.

(2) Xia, F.; Wang, H.; Jia, Y. Rediscovering Black Phosphorus as an Anisotropic Layered Material for Optoelectronics and Electronics. *Nat. Commun.* **2014**, *5* (1), 4458.
(3) Berger, C.; Song, Z.; Li, T.; Li, X.; Ogbazghi, A. Y.; Feng, R.; Dai, Z.; Marchenkov, A. N.; Conrad, E. H.; First, P. N.; de Heer, W. A. Ultrathin Epitaxial Graphite: 2D Electron Gas Properties and a Route toward Graphene-Based Nanoelectronics. *J. Phys. Chem. B* **2004**, *108* (52), 19912−19916.
(4) Butler, S. Z.; Hollen, S. M.; Cao, L.; Cui, Y.; Gupta, J. A.; Gutiérrez, H. R.; Heinz, T. F.; Hong, S. S.; Huang, J.; Ismach, A. F.; Johnston-Halperin, E.; Kuno, M.; Plashnitsa, V. V.; Robinson, R. D.; Ruoff, R. S.; Salahuddin, S.; Shan, J.; Shi, L.; Spencer, M. G.; Terrones, M.; Windl, W.; Goldberger, J. E. Progress, Challenges, and Opportunities in Two-Dimensional Materials Beyond Graphene. *ACS Nano* **2013**, *7* (4), 2898−2926.
(5) Jariwala, D.; Sangwan, V. K.; Lauhon, L. J.; Marks, T. J.; Hersam, M. C. Emerging Device Applications for Semiconducting Two-Dimensional Transition Metal Dichalcogenides. *ACS Nano* **2014**, *8* (2), 1102−1120.
(6) Schwierz, F.; Pezoldt, J.; Granzner, R. Two-Dimensional Materials and Their Prospects in Transistor Electronics. *Nanoscale* **2015**, *7* (18), 8261−8283.
(7) Wang, Q. H.; Kalantar-Zadeh, K.; Kis, A.; Coleman, J. N.; Strano, M. S. Electronics and Optoelectronics of Two-Dimensional Transition Metal Dichalcogenides. *Nat. Nanotechnol.* **2012**, *7* (11), 699−712.
(8) Ithurria, S.; Tessier, M. D.; Mahler, B.; Lobo, R. P. S. M.; Dubertret, B.; Efros, Al. L. Colloidal Nanoplatelets with Two-Dimensional Electronic Structure. *Nat. Mater.* **2011**, *10* (12), 936−941.
(9) Christodoulou, S.; Climente, J. I.; Planelles, J.; Brescia, R.; Prato, M.; Martín-García, B.; Khan, A. H.; Moreels, I. Chloride-Induced Thickness Control in CdSe Nanoplatelets. *Nano Lett.* **2018**, *18* (10), 6248−6254.
(10) Cho, W.; Kim, S.; Coropceanu, I.; Srivastava, V.; Diroll, B. T.; Hazarika, A.; Fedin, I.; Galli, G.; Schaller, R. D.; Talapin, D. V. Direct Synthesis of Six-Monolayer (1.9 nm) Thick Zinc-Blende CdSe Nanoplatelets Emitting at 585 nm. *Chem. Mater.* **2018**, *30* (20), 6957−6960.
(11) Delikanli, S.; Yu, G.; Yeltik, A.; Bose, S.; Erdem, T.; Yu, J.; Erdem, O.; Sharma, M.; Sharma, V. K.; Quliyeva, U.; Shendre, S.; Dang, C.; Zhang, D. H.; Sum, T. C.; Fan, W.; Demir, H. V. Ultrathin Highly Luminescent Two-Monolayer Colloidal CdSe Nanoplatelets. *Adv. Funct. Mater.* **2019**, *29* (35), 1901028.
(12) Akkerman, Q. A.; Motti, S. G.; Srimath Kandada, A. R.; Mosconi, E.; D'Innocenzo, V.; Bertoni, G.; Marras, S.; Kamino, B. A.; Miranda, L.; De Angelis, F.; Petrozza, A.; Prato, M.; Manna, L. Solution Synthesis Approach to Colloidal Cesium Lead Halide Perovskite Nanoplatelets with Monolayer-Level Thickness Control. *J. Am. Chem. Soc.* **2016**, *138* (3), 1010−1016.
(13) Bohn, B. J.; Tong, Y.; Gramlich, M.; Lai, M. L.; Döblinger, M.; Wang, K.; Hoye, R. L. Z.; Müller-Buschbaum, P.; Stranks, S. D.; Urban, A. S.; Polavarapu, L.; Feldmann, J. Boosting Tunable Blue Luminescence of Halide Perovskite Nanoplatelets through Postsynthetic Surface Trap Repair. *Nano Lett.* **2018**, *18* (8), 5231−5238.
(14) Antanovich, A.; Achstein, A. W.; Matsukovich, A.; Prudnikau, A.; Bhaskar, P.; Gurin, V.; Molinari, M.; Artemyev, M. A Strain-Induced Exciton Transition Energy Shift in CdSe Nanoplatelets: The Impact of an Organic Ligand Shell. *Nanoscale* **2017**, *9* (45), 18042−18053.
(15) Dufour, M.; Qu, J.; Greboval, C.; Méthivier, C.; Lhuillier, E.; Ithurria, S. Halide Ligands To Release Strain in Cadmium Chalcogenide Nanoplatelets and Achieve High Brightness. *ACS Nano* **2019**, *13* (5), 5326−5334.
(16) Diroll, B. T.; Schaller, R. D. Shape-Selective Optical Transformations of CdSe Nanoplatelets Driven by Halide Ion Ligand Exchange. *Chem. Mater.* **2019**, *31* (9), 3556−3563.
(17) Diroll, B. T. Ligand-Dependent Tuning of Interband and Intersubband Transitions of Colloidal CdSe Nanoplatelets. *Chem. Mater.* **2020**, *32* (13), 5916−5923.
(18) Ithurria, S.; Talapin, D. V. Colloidal Atomic Layer Deposition (c-ALD) Using Self-Limiting Reactions at Nanocrystal Surface Coupled to Phase Transfer between Polar and Nonpolar Media. *J. Am. Chem. Soc.* **2012**, *134* (45), 18585−18590.
(19) Mahler, B.; Nadal, B.; Bouet, C.; Patriarche, G.; Dubertret, B. Core/Shell Colloidal Semiconductor Nanoplatelets. *J. Am. Chem. Soc.* **2012**, *134* (45), 18591−18598.
(20) Polovitsyn, A.; Dang, Z.; Movilla, J. L.; Martín-García, B.; Khan, A. H.; Bertrand, G. H. V.; Brescia, R.; Moreels, I. Synthesis of Air-Stable CdSe/ZnS Core−Shell Nanoplatelets with Tunable Emission Wavelength. *Chem. Mater.* **2017**, *29* (13), 5671−5680.
(21) Tenne, R.; Pedetti, S.; Kazes, M.; Ithurria, S.; Houben, L.; Nadal, B.; Oron, D.; Dubertret, B. From Dilute Isovalent Substitution to Alloying in CdSeTe Nanoplatelets. *Phys. Chem. Chem. Phys.* **2016**, *18* (22), 15295−15303.
(22) Kelestemur, Y.; Dede, D.; Gungor, K.; Usanmaz, C. F.; Erdem, O.; Demir, H. V. Alloyed Heterostructures of $CdSe_xS_{1-x}$ Nanoplatelets with Highly Tunable Optical Gain Performance. *Chem. Mater.* **2017**, *29* (11), 4857−4865.
(23) Tessier, M. D.; Javaux, C.; Maksimovic, I.; Loriette, V.; Dubertret, B. Spectroscopy of Single CdSe Nanoplatelets. *ACS Nano* **2012**, *6* (8), 6751−6758.
(24) Yeltik, A.; Delikanli, S.; Olutas, M.; Kelestemur, Y.; Guzelturk, B.; Demir, H. V. Experimental Determination of the Absorption Cross-Section and Molar Extinction Coefficient of Colloidal CdSe Nanoplatelets. *J. Phys. Chem. C* **2015**, *119* (47), 26768−26775.
(25) Achtstein, A. W.; Antanovich, A.; Prudnikau, A.; Scott, R.; Woggon, U.; Artemyev, M. Linear Absorption in CdSe Nanoplates: Thickness and Lateral Size Dependency of the Intrinsic Absorption. *J. Phys. Chem. C* **2015**, *119* (34), 20156−20161.
(26) She, C.; Fedin, I.; Dolzhnikov, D. S.; Dahlberg, P. D.; Engel, G. S.; Schaller, R. D.; Talapin, D. V. Red, Yellow, Green, and Blue Amplified Spontaneous Emission and Lasing Using Colloidal CdSe Nanoplatelets. *ACS Nano* **2015**, *9* (10), 9475−9485.
(27) Li, Q.; Lian, T. Area- and Thickness-Dependent Biexciton Auger Recombination in Colloidal CdSe Nanoplatelets: Breaking the "Universal Volume Scaling Law". *Nano Lett.* **2017**, *17* (5), 3152−3158.
(28) Zhang, F.; Wang, S.; Wang, L.; Lin, Q.; Shen, H.; Cao, W.; Yang, C.; Wang, H.; Yu, L.; Du, Z.; Xue, J.; Li, L. S. Super Color Purity Green Quantum Dot Light-Emitting Diodes Fabricated by Using CdSe/CdS Nanoplatelets. *Nanoscale* **2016**, *8* (24), 12182−12188.
(29) Liu, B.; Altintas, Y.; Wang, L.; Shendre, S.; Sharma, M.; Sun, H.; Mutlugun, E.; Demir, H. V. Record High External Quantum Efficiency of 19.2% Achieved in Light-Emitting Diodes of Colloidal Quantum Wells Enabled by Hot-Injection Shell Growth. *Adv. Mater.* **2020**, *32* (8), 1905824.
(30) Guzelturk, B.; Kelestemur, Y.; Olutas, M.; Delikanli, S.; Demir, H. V. Amplified Spontaneous Emission and Lasing in Colloidal Nanoplatelets. *ACS Nano* **2014**, *8* (7), 6599−6605.
(31) Meyer, J. R.; Bartoli, F. J.; Kruer, M. R. Optical Heating in Semiconductors. *Phys. Rev. B: Condens. Matter Mater. Phys.* **1980**, *21* (4), 1559−1568.
(32) Sadasivam, S.; Chan, M. K. Y.; Darancet, P. Theory of Thermal Relaxation of Electrons in Semiconductors. *Phys. Rev. Lett.* **2017**, *119* (13), 136602.
(33) Kirschner, M. S.; Hannah, D. C.; Diroll, B. T.; Zhang, X.; Wagner, M. J.; Hayes, D.; Chang, A. Y.; Rowland, C. E.; Lethiec, C. M.; Schatz, G. C.; Chen, L. X.; Schaller, R. D. Transient Melting and Recrystallization of Semiconductor Nanocrystals Under Multiple Electron−Hole Pair Excitation. *Nano Lett.* **2017**, *17* (9), 5314−5320.
(34) Kirschner, M. S.; Diroll, B. T.; Guo, P.; Harvey, S. M.; Helweh, W.; Flanders, N. C.; Brumberg, A.; Watkins, N. E.; Leonard, A. A.; Evans, A. M.; Wasielewski, M. R.; Dichtel, W. R.; Zhang, X.; Chen, L. X.; Schaller, R. D. Photoinduced, Reversible Phase Transitions in All-Inorganic Perovskite Nanocrystals. *Nat. Commun.* **2019**, *10*, 504.
(35) Kirschner, M. S.; Diroll, B. T.; Brumberg, A.; Leonard, A. A.; Hannah, D. C.; Chen, L. X.; Schaller, R. D. Optical Signatures of Transiently Disordered Semiconductor Nanocrystals. *ACS Nano* **2018**, *12* (10), 10008−10015.

https://dx.doi.org/10.1021/acs.nanolett.0c03958
Nano Lett. 2021, 21, 1288−1294

(36) Ong, W.-L.; Rupich, S. M.; Talapin, D. V.; McGaughey, A. J. H.; Malen, J. A. Surface Chemistry Mediates Thermal Transport in Three-Dimensional Nanocrystal Arrays. *Nat. Mater.* **2013**, *12* (5), 410−415.
(37) Goldstein, A. N.; Echer, C. M.; Alivisatos, A. P. Melting in Semiconductor Nanocrystals. *Science* **1992**, *256* (5062), 1425−1427.
(38) Liu, M.; Wang, R. Y. Size-Dependent Melting Behavior of Colloidal In, Sn and Bi Nanocrystals. *Sci. Rep.* **2015**, *5*, 16353.
(39) Robinson, I. Nanoparticle Structure by Coherent X-Ray Diffraction. *J. Phys. Soc. Jpn.* **2013**, *82* (2), 021012.
(40) Barnard, A. S.; Zapol, P. A Model for the Phase Stability of Arbitrary Nanoparticles as a Function of Size and Shape. *J. Chem. Phys.* **2004**, *121* (9), 4276−4283.
(41) Rowland, C. E.; Fedin, I.; Diroll, B. T.; Liu, Y.; Talapin, D. V.; Schaller, R. D. Elevated Temperature Photophysical Properties and Morphological Stability of CdSe and CdSe/CdS Nanoplatelets. *J. Phys. Chem. Lett.* **2018**, *9* (2), 286−293.
(42) Mannebach, E. M.; Li, R.; Duerloo, K.-A.; Nyby, C.; Zalden, P.; Vecchione, T.; Ernst, F.; Reid, A. H.; Chase, T.; Shen, X.; Weathersby, S.; Hast, C.; Hettel, R.; Coffee, R.; Hartmann, N.; Fry, A. R.; Yu, Y.; Cao, L.; Heinz, T. F.; Reed, E. J.; Dürr, H. A.; Wang, X.; Lindenberg, A. M. Dynamic Structural Response and Deformations of Monolayer MoS_2 Visualized by Femtosecond Electron Diffraction. *Nano Lett.* **2015**, *15* (10), 6889−6895.
(43) Tung, I.-C.; Krishnamoorthy, A.; Sadasivam, S.; Zhou, H.; Zhang, Q.; Seyler, K. L.; Clark, G.; Mannebach, E. M.; Nyby, C.; Ernst, F.; Zhu, D.; Glownia, J. M.; Kozina, M. E.; Song, S.; Nelson, S.; Kumazoe, H.; Shimojo, F.; Kalia, R. K.; Vashishta, P.; Darancet, P.; Heinz, T. F.; Nakano, A.; Xu, X.; Lindenberg, A. M.; Wen, H. Anisotropic Structural Dynamics of Monolayer Crystals Revealed by Femtosecond Surface X-Ray Scattering. *Nat. Photonics* **2019**, *13* (6), 425−430.
(44) Hu, J.; Vanacore, G. M.; Cepellotti, A.; Marzari, N.; Zewail, A. H. Rippling Ultrafast Dynamics of Suspended 2D Monolayers, Graphene. *Proc. Natl. Acad. Sci. U. S. A.* **2016**, *113* (43), E6555−E6561.
(45) Miró, P.; Ghorbani-Asl, M.; Heine, T. Spontaneous Ripple Formation in MoS_2 Monolayers: Electronic Structure and Transport Effects. *Adv. Mater.* **2013**, *25* (38), 5473−5475.
(46) Shcherbinin, S. A.; Zhou, K.; Dmitriev, S. V.; Korznikova, E. A.; Davletshin, A. R.; Kistanov, A. A. Two-Dimensional Black Phosphorus Carbide: Rippling and Formation of Nanotubes. *J. Phys. Chem. C* **2020**, *124* (18), 10235−10243.
(47) Jurgilaitis, A.; Enquist, H.; Andreasson, B. P.; Persson, A. I. H.; Borg, B. M.; Caroff, P.; Dick, K. A.; Harb, M.; Linke, H.; Nüske, R.; Wernersson, L.-E.; Larsson, J. Time-Resolved X-Ray Diffraction Investigation of the Modified Phonon Dispersion in InSb Nanowires. *Nano Lett.* **2014**, *14* (2), 541−546.
(48) Wittenberg, J. S.; Miller, T. A.; Szilagyi, E.; Lutker, K.; Quirin, F.; Lu, W.; Lemke, H.; Zhu, D.; Chollet, M.; Robinson, J.; Wen, H.; Sokolowski-Tinten, K.; Alivisatos, A. P.; Lindenberg, A. M. Real-Time Visualization of Nanocrystal Solid−Solid Transformation Pathways. *Nano Lett.* **2014**, *14* (4), 1995−1999.
(49) Szilagyi, E.; Wittenberg, J. S.; Miller, T. A.; Lutker, K.; Quirin, F.; Lemke, H.; Zhu, D.; Chollet, M.; Robinson, J.; Wen, H.; Sokolowski-Tinten, K.; Lindenberg, A. M. Visualization of Nanocrystal Breathing Modes at Extreme Strains. *Nat. Commun.* **2015**, *6* (1), 6577.
(50) Harvey, S. M.; Houck, D. W.; Kirschner, M. S.; Flanders, N. C.; Brumberg, A.; Leonard, A. A.; Watkins, N. E.; Chen, L. X.; Dichtel, W. R.; Zhang, X.; Korgel, B. A.; Wasielewski, M. R.; Schaller, R. D. Transient Lattice Response upon Photoexcitation in $CuInSe_2$ Nanocrystals with Organic or Inorganic. *ACS Nano* **2020**, *14* (10), 13548−13556.
(51) Li, Z.; Peng, X. Size/Shape-Controlled Synthesis of Colloidal CdSe Quantum Disks: Ligand and Temperature Effects. *J. Am. Chem. Soc.* **2011**, *133* (17), 6578−6586.
(52) Chen, D.; Gao, Y.; Chen, Y.; Ren, Y.; Peng, X. Structure Identification of Two-Dimensional Colloidal Semiconductor Nanocrystals with Atomic Flat Basal Planes. *Nano Lett.* **2015**, *15* (7), 4477−4482.
(53) Tomar, R.; Kulkarni, A.; Chen, K.; Singh, S.; van Thourhout, D.; Hodgkiss, J. M.; Siebbeles, L. D. A.; Hens, Z.; Geiregat, P. Charge Carrier Cooling Bottleneck Opens Up Nonexcitonic Gain Mechanisms in Colloidal CdSe Quantum Wells. *J. Phys. Chem. C* **2019**, *123* (14), 9640−9650.

https://dx.doi.org/10.1021/acs.nanolett.0c03958
Nano Lett. 2021, 21, 1288−1294